1992ApJ...395..347B

THE ASTROPHYSICAL JOURNAL, 395:347–359, 1992 August 20
© 1992. The American Astronomical Society. All rights reserved. Printed in U.S.A.

THE VELOCITY-DISTANCE RELATION FOR GALAXIES ON A BUBBLE

GREGORY D. BOTHUN[1]
Department of Physics, University of Oregon, Eugene, OR 97403
AND
MARGARET J. GELLER,[1] MICHAEL J. KURTZ, JOHN P. HUCHRA, AND RUDOLPH E. SCHILD
Harvard-Smithsonian Center for Astrophysics, 60 Garden Street, Cambridge, MA 02138
Received 1991 August 28; accepted 1992 February 27

ABSTRACT

We use the *I*-band Tully-Fisher (TF) relation to measure relative distances to galaxies on the edges of the largest (~ 5000 km s^{-1}) void in the first slice of the Center for Astrophysics redshift survey extension. We divide the data into three samples: H (seven galaxies) on the high-velocity edge of the void, L (10 galaxies) along the low-velocity edge, and P (nine galaxies) distributed nearly along the line of sight adjacent to the Coma cluster. We show that sample P is infalling toward Coma. For samples H and L the scatter about the Hubble diagram is $0^m.18$, comparable with the error in an individual *I*-band TF measurement.

The ratio of *I*-band TF distances to the high- and low-velocity boundaries (samples H and L) is $2.22^{+0.11}_{-0.10}$ and the ratio of velocities is 2.16 ± 0.08. In other words, to within the error the void has the same diameter in real and redshift space.

The mean peculiar velocity of sample L is 32 ± 108 km s^{-1}; for sample H it is -113 ± 253 km s^{-1}. In other words, the data are consistent with no outflow from the void and the 1 σ upper limit to outflow from the void is $\sim 5\%$ of the void diameter. For a simple model, the 2 σ limits on the outflow yield $\Omega \lesssim 1$.

We detect the "infall" of sample P toward Coma at better than the 3 σ level: the line-of-sight component of the infall is 915 ± 263 km s^{-1} at a distance of 26 h^{-1} Mpc ($H_0 = 100\ h$ km s^{-1} Mpc^{-1}) from the center of the Coma cluster. For spherically symmetric infall, the implied value of $\Omega = 2.2^{+2.0}_{-2}$; the 2 σ error includes only the error in the infall measurement and ignores the large error in the extrapolated density of the Coma cluster.

Subject headings: galaxies: clustering — galaxies: distances and redshifts — MHD

1. INTRODUCTION

Large-redshift surveys reveal striking coherent structures in the large-scale distribution of galaxies. One clear example is the cellular distribution of galaxies in the redshift survey of de Lapparent et al. (1986, hereafter SLICE). The distribution contains voids with diameters as large as 50 h^{-1} Mpc, and with sharp, dense edges. This rich, complex structure in the distribution of light-emitting matter is a profound theoretical challenge. Theories must reproduce the observed structure: the large-scale end of the distribution of void sizes is particularly challenging.

Proponents of cold dark matter (CDM) (White et al. 1987; Park 1990; Weinberg & Gunn 1990), hot dark matter (HDM) (Centrella et al. 1988; Cen 1991) and explosion models (Cowie & Ostriker 1981; Ikeuchi 1981) *qualitatively* reproduce some aspects of the structure in the SLICE and in the more extensive data set of Geller & Huchra (1989). On the largest scales, the models do not yet provide an adequate match to the data (Saunders et al. 1991). To account for both large-scale coherent structures in the distribution of light-emitting matter and extraordinary smoothness of the cosmic microwave background (see Readhead et al. 1989), all of these models demand that the distribution of light be decoupled from the distribution of mass.

Redshift surveys alone provide inadequate constraints on the relative distribution of dark and light-emitting matter. Distance determinations for substantial samples of galaxies in regions where there are complete redshift surveys can vastly increase the discriminatory power of the data. With the improvement in distance determinations to individual galaxies offered by the *H*-band Tully-Fisher relation (Aaronson et al. 1989), the CCD *I*-band TF relation (Bothun & Mould 1987; Pierce & Tully 1988), and the surface brightness corrected Faber-Jackson relation (Burstein et al. 1987), it is now possible to measure the peculiar velocities (i.e., deviations from Hubble Flow) of individual galaxies.

Mapping of the peculiar velocity field constrains a combination of the large-scale matter density contrast and the cosmological density parameter Ω. Measurements of peculiar velocities combined with estimates of the matter density contrast can then yield an estimate of Ω (e.g., Regös & Geller 1989). Examples of this approach include studies of Virgocentric flow (Tonry & Davis 1981; Aaronson et al. 1982; Yahil 1985; Villumsen & Davis 1986), the flow induced by the "Great Attractor" (Lynden-Bell et al. 1988; Aaronson et al. 1989), and the infall patterns associated with rich clusters (Regös & Geller 1989). All of these studies suggest that $0.1 \lesssim \Omega \lesssim 1$.

Just as matter flows toward overdense regions, it flows out of underdense regions. Because a void is presumably a region where the matter density is substantially lower than in the surroundings, we expect a net flow outward from the center of the void. The amplitude of this outflow depends upon Ω. To determine the outflow velocity it is necessary to derive relative distances between galaxies located on the near and far edges of

[1] Guest Observers at the National Astronomy and Ionosphere Center operated by Cornell University under a cooperative agreement with the National Science Foundation.

© American Astronomical Society • Provided by the NASA Astrophysics Data System

1992ApJ...395..347B

the void. By comparing the dimensions of the bubble in physical space with those inferred from the near-to-far redshift, we can contrain the outflow velocity.

In this paper, we measure the characteristic diameter of the most prominent void in the SLICE. We use the Tully-Fisher relation to determine distances to individual galaxies. Velocity widths come from 21 cm observations and luminosities come from CCD *I*-band observations. Freudling, Haynes, & Giovanelli (1988) used the Tully-Fisher relation in the blue (where the scatter is larger) to investigate the dynamics of this region. Their data cover a larger volume more sparsely. They conclude that the outflow velocity is $\lesssim 10\%$ of the void diameter.

Section 2 describes our data. In § 3 we derive distances and peculiar velocities to individual galaxies. We show that the void is approximately a "Hubble Bubble": the near and far edges are separating with the general expansion of the universe. At the 3 σ level, we also detect infall toward the Coma cluster for a portion of the bubble wall. We use the limits on the net outflow from the void and infall into Coma to estimate Ω. Our conclusions are presented in § 4.

2. OBSERVATIONS

2.1. *Sample Selection*

One of the largest voids in the CfA survey (Geller & Huchra 1989) lies in the right ascension range $13^h.2 \lesssim \alpha \lesssim 17^h$. The eastern boundary of the void lies outside the right ascension range of the survey (which is limited by the Galactic plane, but see Marzske et al. 1992 for an extension of the survey across the plane). In declination, the void appears over the range $26°.5 \leq \delta < 44°.5$; again its boundaries are outside the declination coverage of the complete survey. We selected galaxies for *I*-band TF distance measurements from the first complete slice of the CfA survey which covers the declination range $26°.5 \leq \delta < 32°.5$. The galaxies in the sample are in the right ascension range $13^h.2 \leq \alpha \leq 15^h.7$. Figure 1 is a cone diagram for the complete survey in the region for galaxies with redshifts $\leq 10{,}000$ km s^{-1}. The diameter of the void in redshift space is ~ 5000 km s^{-1}.

The CfA survey, and hence our sample, include galaxies with $m_{\rm Zwicky} \leq 15.5$. The scatter and possible systematic variations in this limit are ~ 0.3 mag. (see Bothun & Cornell 1990). Most of the galaxies in the region we investigate here are spirals (Huchra et al. 1990). In order to apply the Tully-Fisher relation we selected only those galaxies which have at least a 40° inclination relative to the line of sight. Our target sample includes 77 galaxies (Table 1).

2.2. *Observations and Reductions*

We observed these 77 galaxies with the Arecibo 305 m spherical reflector in 1987 June. The observational set-up was identical to that described by Bothun et al. (1985). Because velocities for all 77 galaxies were known (Huchra et al. 1990), we set the LO velocity to the optical velocity and integrated for two consecutive 5 minute ON-OFF pairs before deciding that we either had sufficient signal-to-noise, needed better signal-to-noise, or were not going to detect the galaxy. Overall, we detected 44/77 (57%) of the program galaxies. The detection percentage is a function of redshift: 29/41 (71%) galaxies with velocities ≤ 7000 km s^{-1} were detected compared with 15/36 (42%) of the more distant galaxies. This somewhat lower detection rate reflects the bias in the Zwicky catalog toward high surface brightness galaxies many of which are relatively early

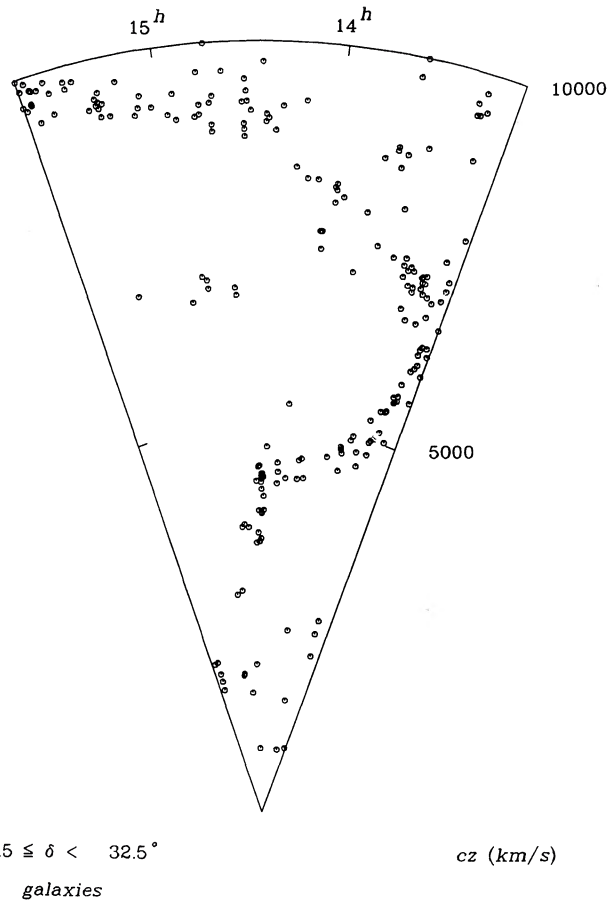

FIG. 1.—Cone diagram for the region $13^h.3 \leq \alpha \leq 17^h$, $26°.5 \leq \delta < 32°.5$, and $cz \leq 10{,}000$ km s^{-1}. The sample (213 galaxies) is magnitude-limited with $m_{B(0)} \leq 15.5$.

Hubble type. Such galaxies generally have H I masses $\leq 10^9$ $M_\odot$ and hence are difficult to detect beyond velocities of ≈ 5000 km s^{-1}, particularly when they are edge on and the signal is spread out over several hundred km s^{-1}. Indeed, the morphology on the CCD frames of most of the undetected galaxies is consistent with S0–Sab Hubble type. Table 1 includes all galaxies in the sample. The table includes nondetections, weak detections, galaxies with Gaussian line profiles (indicative of face-on orientation), and the 38 galaxies with measured line-widths. Figure 2 shows the H I profiles of all the detected galaxies.

Freudling et al. (1988) observed seven of these galaxies. The average ratio of line widths $(\text{H I}_{\text{this paper}}/\text{H I}_{\text{Freudling}}) = 1.1 \pm 0.06$. This systematic in line width measurements reflects the difference in convention between Aaronson et al. (1980) and Freudling et al. (1988). Both conventions produce internally consistent TF relations. The average difference in inclination angle $(i_{\text{this paper}} - i_{\text{Freudling}}) = 2° \pm 2°$. The estimated error for a single inclination angle is $\sim 5°$.

We acquired multicolor CCD frames with the 0.6 m telescope of the Whipple observatory. A cooled RCA chip was used as the detector in combination with either the f/6.5 or f/13 secondary. These combinations yield pixel scales of 1".46 and 0".73 pixel^{-1}, respectively. We use the procedure of Bothun & Mould (1987) to do the surface photometry. We use Landolt (1983) standards in SA 108 as well as calibration fields in M67 (Schild 1983) for photometric calibration. For the *I*-band, the

© American Astronomical Society • Provided by the NASA Astrophysics Data System

1992ApJ...395..347B

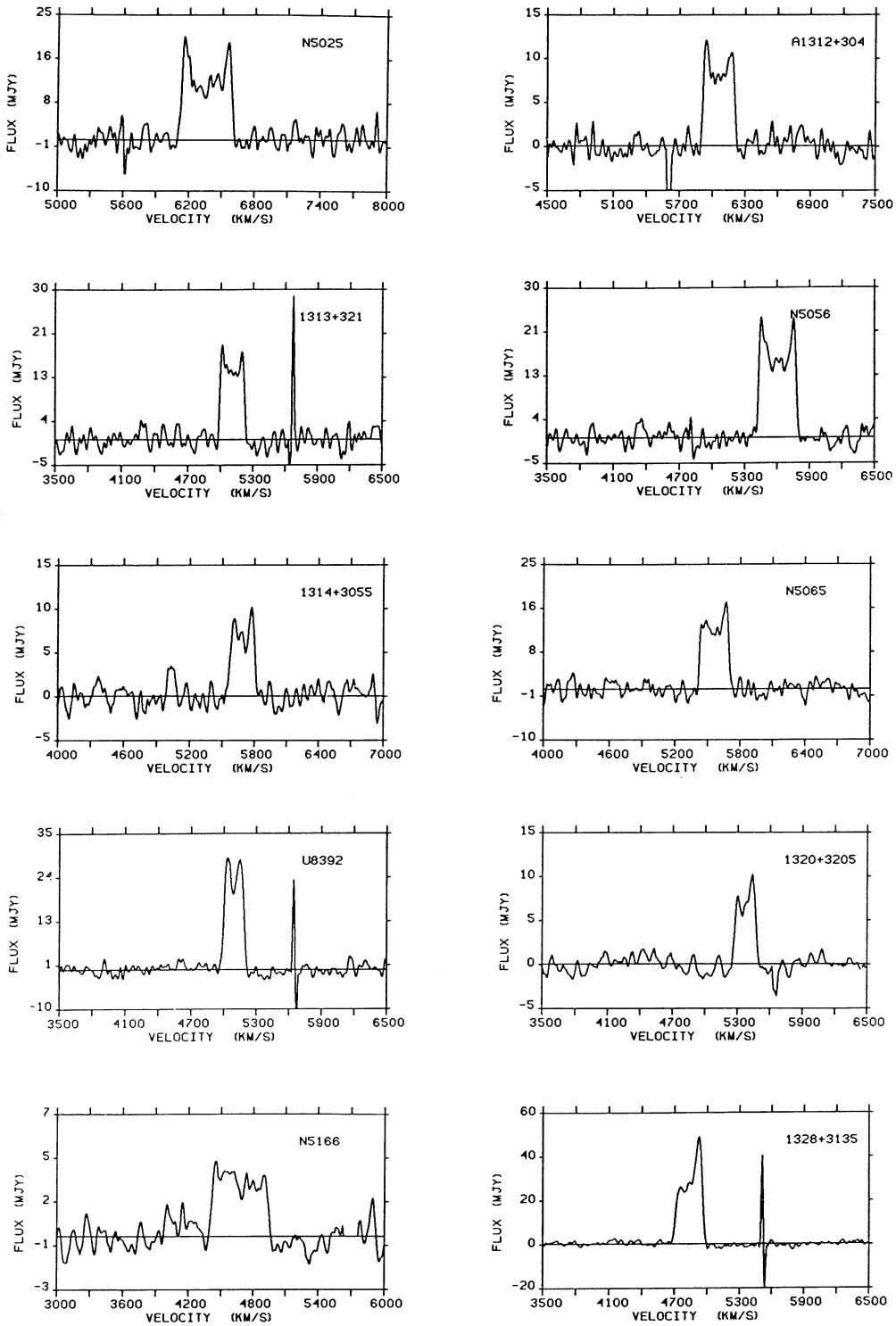

FIG. 2.—21 cm profiles for the 44 detected galaxies. Note that U8392 is 1318+3129 in Table 1.

scatter in photometric zeropoints is 0.025 mag. The $(R-I)$ color term is negligible and the average extinction at I is 0.08 mag per air mass.

Although the f/6.5 resolution is rather coarse for galaxies of only $\sim 1'$ diameter, it is sufficient to define the constant surface brightness ellipses used to determine the total magnitudes. We extract isophotal I-band magnitudes by summing the flux in each fitted ellipse. We determine inclinations from the mean ellipticity of the isophotes in the range $21.0 \leq \mu_i \leq 23.0$ mag arcsec^{-2} and include the 3° additive term of Aaronson et al. (1980). The surface photometry typically reaches a level of $I = 24.0$ mag arcsec^{-2}, which is ~ 5.0 mag below the nominal I-band sky brightness. We determine total I-band magnitudes by extrapolating the elliptical aperture versus magnitude rela-

© American Astronomical Society • Provided by the NASA Astrophysics Data System

1992ApJ...395..347B

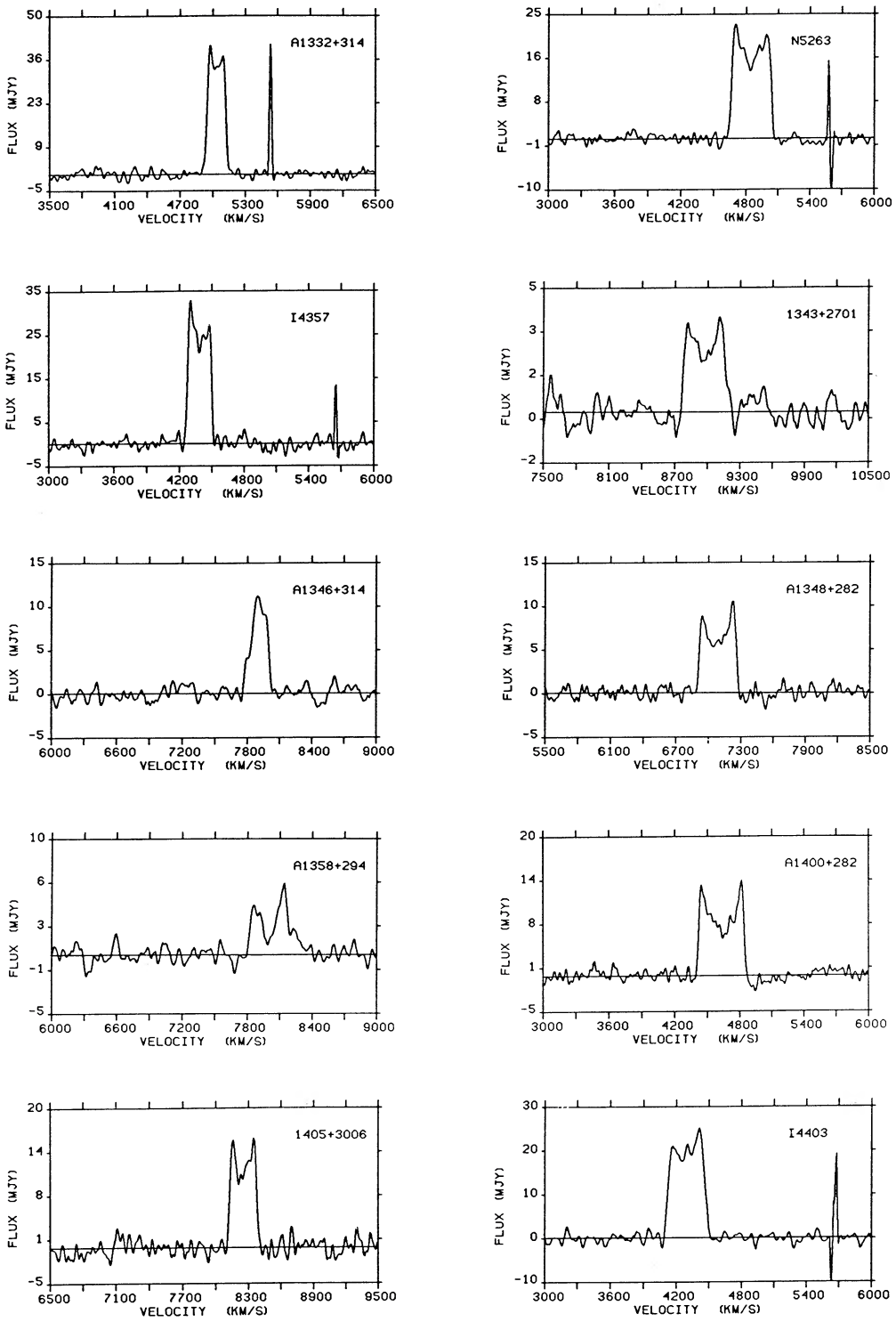

FIG. 2—*Continued*

tion to infinity. For these data, this extrapolation is always ≤ 0.05 mag and is not the major source of uncertainty in the total magnitude.

The major source of uncertainty in the total magnitudes is fluctuation in the sky background in the CCD frame. The sky background in the *I*-band ($\sim$7200–8500 Å) is dominated by OH emission bands. The intensity of these bands is quite variable with time. Because of this variation, it is difficult to obtain a flat-field in which the CCD is illuminated in precisely the same way it was during the galaxy exposure. Errors in the sky background are especially important at *I* because the sky is substantially brighter than most of the galaxy. Use of the shape of the aperture-magnitude relation minimizes this problem because the relation is weighted by the higher surface bright-

© American Astronomical Society • Provided by the NASA Astrophysics Data System

1992ApJ...395..347B

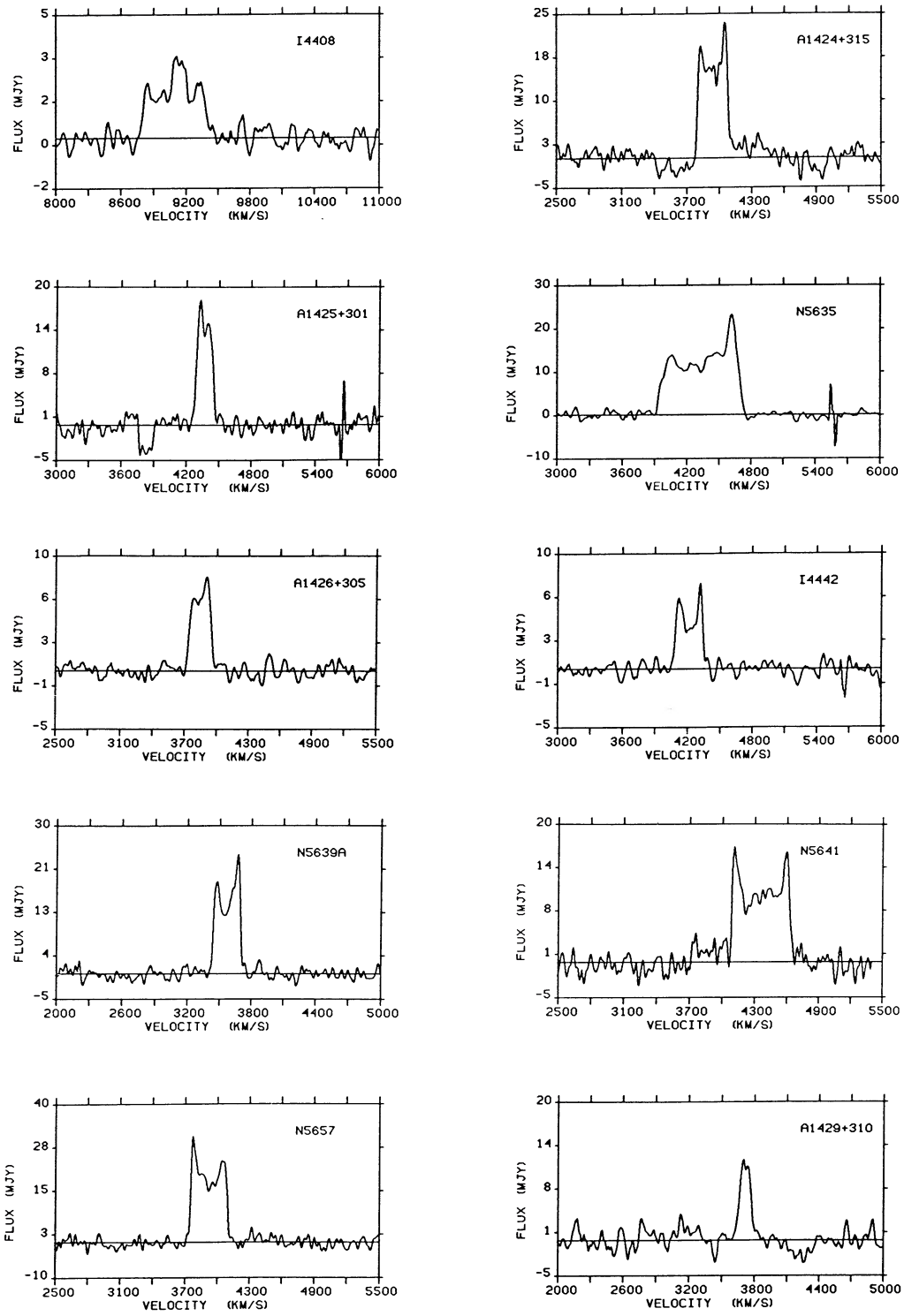

FIG. 2—*Continued*

ness points which are relatively unaffected by errors in the sky background. Experimentation on the images shows that changing the mean sky background by 0.5% leads to errors of 0.08–0.12 mag in the derived total magnitude. For our data, the 1 σ error in sky background ranges from 0.1%–0.4%. Summing the flux inside an elliptical "isophote" larger than the galaxy provides much less stable results because the fit of the outlying ellipse is dominated by fluctuations in the sky background. These fluctuations in the sky background preclude determination of the total magnitude by integrating the surface brightness profile to infinity. The outermost isophotes can have errors as large as 0.5 mag arcsec^{-2}; these errors imply *systematic* errors in the total *I*-band magnitude of 0.05–0.1 mag.

© American Astronomical Society • Provided by the NASA Astrophysics Data System

1992ApJ...395..347B

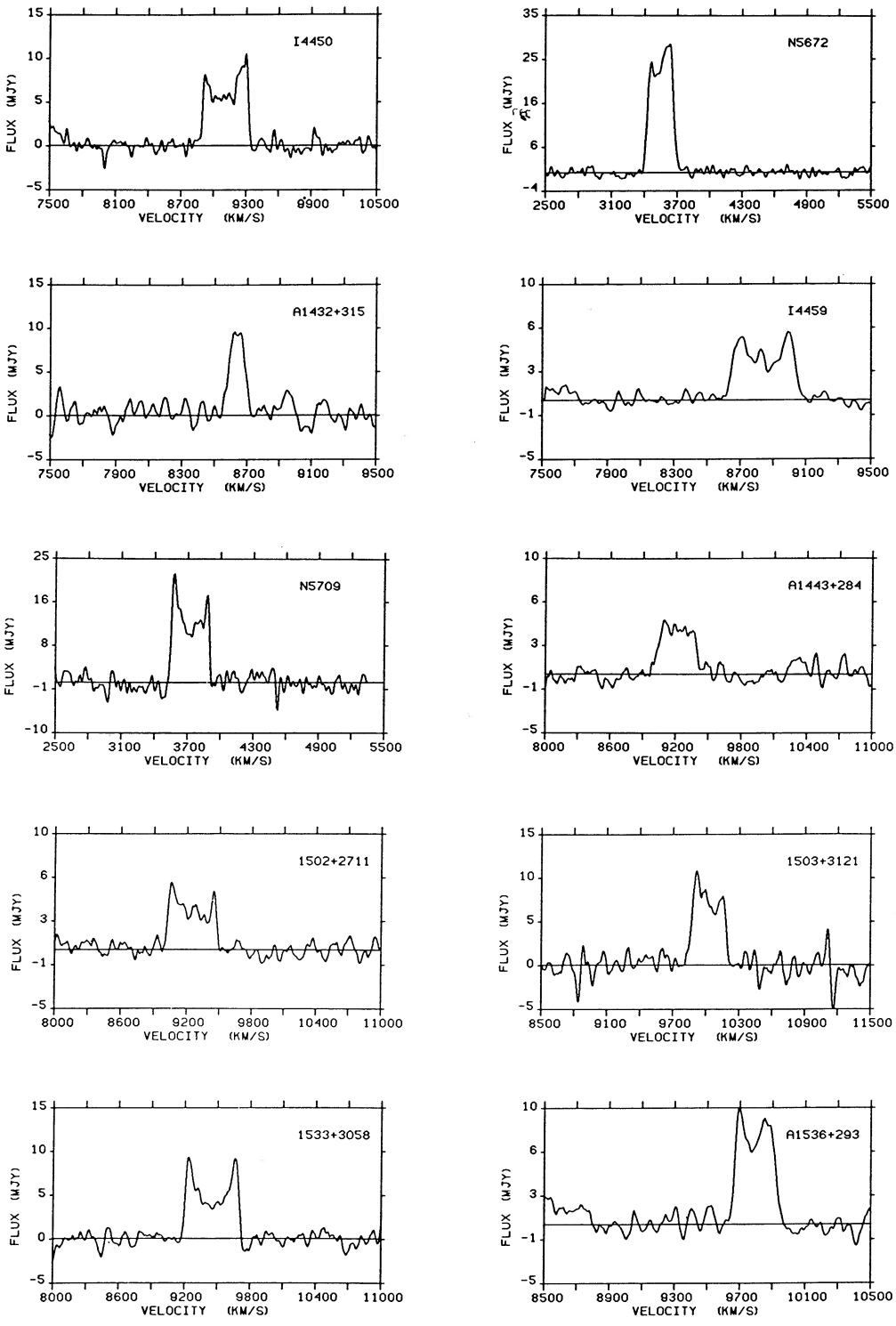

FIG. 2—*Continued*

Bothun & Mould (1987) suggest that surface brightness variations at fixed line width are the largest source of scatter in the TF relation. For galaxies of normal surface brightness, our surface photometry detects 4 scale lengths of disk light which represents 90% of the total luminosity. However, there are galaxies with similar line width but with central surface brightnesses at least 2 mag fainter (e.g., Schombert et al. 1992). For these galaxies, our surface photometry would cover only 2 scale lengths of disk light (e.g., 59% of the total light) and the galaxy would be well displaced below the nominal TF relation. In our data, there is very little scatter in surface brightness at fixed line width. This limited range in surface brightness is a consequence of selecting galaxies exclusively from the Zwicky catalog. We can thus substitute our more accurate isophotal

© American Astronomical Society • Provided by the NASA Astrophysics Data System

1992ApJ...395..347B

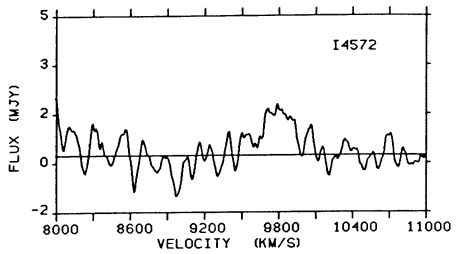

FIG. 2—*Continued*

magnitudes for the less certain total magnitudes to produce an internally consistent *I*-band TF relation. The use of these accurate isophotal magnitudes coupled with the relatively high signal-to-noise of the H I detections (see Fig. 2) yields *I*-band TF relations with a scatter of less than 0.2 mag (see also Freedman 1990).

Table 1 contains the basic observational data for the galaxies with measured H I line widths. Column (1) lists the galaxy name and columns (2) and (3) gives its right ascension and declination. Column (4) refers to the subsamples we analyze below. Columns (5) and (6) list the telescope optics and exposure time (in minutes) for the CCD observations. Column (7) lists the total *I*-band magnitude, uncorrected for reddening. Column (8) contains the reddening corrected isophotal magnitude within the $I = 22.5$ mag arcsec^{-2} isophote (Bothun & Mould 1987). Column (9) gives the internal reddening determined according to Bothun et al. (1985). We assume the reddening in the Cousins *I*-band is 0.42 that at *B*. Columns (10) and (11) list the observed 20% line width and its error (calculated according to Bothun et al. 1985). Column (12) gives the observed line width divided by $(1 + z)$ and corrected for the inclination in column (15). Columns (13) and (14) list the heliocentric 21 cm and optical redshifts, respectively. Column (16) gives the 21 cm flux integral. Column (17) contains comments.

One potential complication in the determination of true isophotal magnitudes is the unknown relation between scattering/absorption of starlight by dust versus enhanced surface brightness due to increasing pass length through the disk (see also Boroson 1981). Some workers have suggested that disk galaxies are optically thick (e.g., Disney, Davies, & Phillips 1989; Valentjin 1990) in which case there is no relation between surface brightness and inclination. Other investigators (e.g., Witt, Thronson, & Capuano 1991; Bothun & Rogers 1992) have shown that disk galaxies are likely to be optically thin at all wavelengths. Witt et al. (1991), in particular, show that forward scattering by dust is very important and hence disk galaxies are unlikely to be ever dimmed by more than $A_B = 1$ mag. Because our sample of disk galaxies, as do most other samples, form a coherent Tully-Fisher relation with relatively low scatter, it is unlikely that variations in optical depth are significant. Hence, in the determination of isophotal magnitudes, we assume that disk galaxies are optically thin and correct the isophotes for modest reddening according to the convention of Bothun et al. (1985).

2.3. *The Anamolous Galaxy NGC 5635*

Except for NGC 5635, none of the galaxies listed in Table 1 have exceptional properties. This galaxy is of early type (Sb) but contains a large amount of H I. The rotation velocity, 430 km s^{-1} (after correction for inclination and redshift) is one of the largest ever observed and substantially exceeds the range of V_{max} over which the slope of the TF relation has been measured. The most luminous Sa galaxies in the sample of Rubin et al. (1985) have rotation velocities of 370 km s^{-1}, and the galaxy UGC 12591 which holds the current record (e.g., Giovanelli et al. 1986) has a rotation velocity of 500 km s^{-1}.

A deconvolution of the surface brightness profile into bulge and disk components yields a disk scale length of 4.1 ± 0.3 kpc, similar to our Galaxy. Using the total *I*-band magnitude and an assumed $B-I$ color of 2.3 for a galaxy of this morphological type yields an *indicative* $(M/L)_B$ of ~ 35, much larger than the value of 5–10 which is typical for spiral galaxies. NGC 5635 is significantly underluminous for its line width (compared to the rest of the sample). As we would expect, its position in the Tully Fisher relation is highly discrepant with respect to a linear extrapolation of the *I*-band TF relation.

3. DISTANCES TO GALAXIES ON A BUBBLE

Based on the redshift survey in the region (Fig. 1), we define the subsamples we use to examine the large-scale velocity field. We then use the *I*-band TF distances to derive a photometric diameter for the void. We compare the photometric diameter with the diameter in redshift space to set a limit on the outflow from the low-density region. The data also provide a measurement of the infall velocity toward the Coma cluster. We use the infall toward Coma to set a limit on Ω on a scale of $\sim 26\ h^{-1}$ Mpc.

3.1. *Definition of Subsamples for Analysis of the Velocity Field*

Table 1 contains 38 galaxies with measured line widths. Thirty-five of these have *I*-band photometry and yield TF distances. *Before* analyzing the velocity field, we throw out eight of the galaxies. We eliminate N5635 because of its anomalously large line width (see § 2.3). We discard N5672, 1426+3051, 1332+3141, N5065, 1318+3129, 1536+2935a, and I4408 based on the comments in column (17) of Table 1. For these galaxies, ΔV_c is unreliable because of interaction, confusion in the 21 cm beam or poorly determined inclination.

In order to analyze the flow pattern, we need a reference system. The choice of a system is complicated because there is no absolute calibration for our I-band Tully-Fisher relation. Because we use isophotal rather than total magnitudes, we cannot use the data of Pierce & Tully (1988) to measure distances relative to Virgo. We measure only *relative* distances. We can thus measure the relative distance to the high (H) and low (L) redshift boundaries of the void and we can examine flow along the boundary nearly parallel to the line-of-sight (P; $\alpha \leq 13^h.5$). This binning of the sample corresponds to the expected physical situation. We effectively distinguish between objects with line-of-sight motions mostly perpendicular to the observed structure in redshift space (samples H and L) and those with line-of-sight motion primarily along the "wall" in redshift space (sample P). Without this distinction flows along the walls (expected for sample P; see Regös & Geller 1992) could dominate the limits on outflow placed by samples H and L.

We *assume* that, taken together, samples H and L (17 galaxies) are at rest with respect to the microwave background frame (CMB). We transform the heliocentric velocities in Table 1 to the CMB frame using the value for the dipole moment from Halpern et al. (1988): $\alpha = 11^h.3$; $\delta = -7°.7$; $v = 360$ km s^{-1}. Table 2 contains the corrected velocities for the 35 galaxies with *I*-band TF distances. We omit the galaxy 1348+2824 (*) from the definition of the standard of rest

© American Astronomical Society • Provided by the NASA Astrophysics Data System

1992ApJ...395..347B

TABLE 1

GALAXY DATA

(1) Galaxy	(2) α (1950.0)	(3) δ (1950.0)	(4) Samp	(5) Opt	(6) Exp (min)	(7) I_{tot}	(8) I_{iso}	(9) Red	(10) Δυ	(11) $\Delta\upsilon_{err}$	(12) $\Delta\upsilon_c$ (km s^{-1})	(13) υ_{21}	(14) υ_{opt}	(15) Inc (deg)	(16) Flux (Jy km s^{-1})	(17) Comment
I4210	13:08:24	29:59											6426			not detected
N5025	13:10:24	32:04	P	f6.5	12	12.32	12.57	0.24	495	12	492	6346	6346	80	6.2	
1312+3045	13:12:00	30:45	P	f6.5	15	13.33	13.61	0.13	313	6	331	6045	6022	68	2.7	
1313+3206	13:13:24	32:06	P	f6.5	15	13.53	13.79	0.11	250	5	271	5096	5038	65	3.4	
N5056	13:13:48	31:12	P	f6.5	15	11.90	12.28	0.08	379	8	430	5590	5596	60	6.3	bright star nrby., sky uncertain
1314+3055	13:14:00	30:55	P	f6.5	15	13.35	13.71	0.11	253	10	274	5672	5676	65	1.8	
1315+3118	13:15:00	31:18											5581			wiped out by interference
N5065	13:15:12	31:20	–	f13.	15	12.57	12.80	0.06	291	6	348	5547	5550	55	3.5	inc. uncertain
I4225	13:17:42	32:14											5438			not detected
1318+3129	13:18:54	31:29	–	f13.	15	13.60	14.27	0.06	217	5	258	5080	5081	56	4.9	inc. uncertain
1320+3205	13:20:30	32:05	P	f13.	15	14.09	14.43	0.11	224	11	241	5358	5415	66	1.5	
1321+3136	13:21:54	31:26											4979			HI too weak
1324+3228	13:24:36	32:28	P	f6.5	15	12.54	12.74	0.10	392	12	432	5276	5273	63	5.3	HI (Bothun *et al.* 1984)
N5166	13:25:54	32:17	P	f6.5	15	11.64	11.84	0.24	558	20	556	4661	4647	81	1.7	
1328+3135	13:28:00	31:35							285	5		4819	4827		8.1	bad CCD data, interacting gals.
1332+3141	13:31:57	31:41	–	f13.	15	14.65	15.53	0.06	208	3	247	5015	5017	56	6.5	inc. uncertain, distorted gal.
1336+3138	13:13:36	31:38											4533			not detected
1337+3134	13:37:12	31:34											4815			not detected
N5263	13:37:36	28:40	P	f6.5	15	12.17	12.30	0.24	401	5	406	4863	4848	76	6.9	
1339+2721	13:39:27	27:21											8800			not detected
1339+2716	13:39:30	27:16											8750			not detected
1340+3147	13:40:12	31:47											7492			not detected
1343+2701	13:43:36	27:01	H	f13.	15	13.68	13.88	0.11	422	7	452	8977	8629	65	1.1	
1345+3035	13:45:00	30:35											4686			not detected
1346+3143	13:46:18	31:43		f13.	15				243	25		7881	7900		1.8	Gaussian HI profile, face-on
1348+2824	13:48:12	28:24	*	f13.	15	13.26	13.42	0.12	370	6	396	7073	7105	66	2.5	
1358+3019	13:58:30	30:19											8132			not detected
I4357	13:58:30	32:08	L	f13.	15	13.44	13.78	0.08	246	5	280	4372	4367	60	5.9	asymmetric optical gal.
1358+2948	13:58:42	29:48											7964			confused in HI beam
1358+2946	13:58:48	29:46		f13.	15	13.05	13.26	0.06				8040	7964	55	1.4	useless, confusion in HI beam with previous gal.
1400+2816	14:00:42	28:16	L	f6.5	15	12.39	12.46	0.24	447	5	447	4616	4581	80	3.8	very high surface brightness gal.
1402+2809	14:02:18	28:09											4592			face-on detection
1402+3059	14:02:30	30:59											7578			not detected
1402+3118	14:02:36	31:18											4346			HI suspended somewhere in N-sp.
1405+3006	14:05:42	30:06	H	f6.5	12	13.04	13.48	0.02	277	8	470	8236	8238	35	3.2	two Horns, but I < 40
1411+2715	14:11:00	27:15											5309			not detected
1411+2940	14:11:30	29:40											9249			not detected
I4403	14:16:06	31:53	L	f6.5	15	12.28	12.57	0.11	402	10	434	4288	4273	66	7.1	
N5553	14:16:12	26:31											4539			not detected
I4408	14:19:00	30:13	–	f13.	15	12.70	12.85	0.12	500	30	527	9083	9168	67	1.2	two gals. in HI beam, line widths uncertain
I4427	14:24:42	27:06											8960			not detected
1424+3145	14:24:42	31:45	L	f6.5	15	12.87	13.08	0.24	302	8	305	3944	3931	78	5.0	
I1012	14:24:54	31:10											4077			HI too weak
1425+3010	14:25:12	30:10	L	f13.	15	13.97	14.52	0.04	190	7	252	4355	4383	48	2.4	could be more face-on
N5635	14:26:18	27:38	–	f6.5	15	10.81	11.03	0.13	805	12	856	4313	4325	68	9.9	biggest HI line width ever
1426+3051	14:26:24	30:51	–	f13.	15	14.31	14.52	0.15	241	11	253	3832	3890	40	1.4	one-sided gal., nucleus off-ctr.
I4442	14:26:30	29:12	L	f13.	15	13.01	13.36	0.07	284	15	330	4212	4193	58	4.3	
N5639A	14:26:36	30:38	L	f13.	15	12.46	12.71	0.06	291	7	351	3557	3585	55	4.3	
N5641	14:27:06	29:03	L	f6.5	15	10.87	11.06	0.12	569	13	614	4342	4331	66	5.9	
I4447	14:27:06	31:03											4280			not detected
N5657	14:28:30	29:24	L	f13.	15	12.21	12.46	0.18	376	13	390	3916	3911	72	7.2	
1429+3100	14:29:06	31:00		f13.	15	13.86						3700	3629			Gaussian HI, face-on detection
I4450	14:29:54	28:46	H	f13.	15	13.32	13.58	0.10	459	16	496	9096	9102	64	2.9	
N5672	14:30:30	31:53	–	f13.	15	12.70	12.97	0.05	297	3	378	3541	3497	51	6.3	peculiar gal., inc. uncertain
1431+2855	14:31:06	28:55											9226			not detected
1431+2810	14:31:54	28:10											9511			not detected
1432+3146	14:32:12	31:46										8620	8766			Gaussian HI, face-on detection
I4459	14:32:18	31:11	H	f6.5	12	13.69	13.89	0.17	435	15	447	8828	8862	71	1.7	
N5709	14:36:36	30:39	L	f6.5	12	12.27	12.50	0.24	370	7	378	3708	3700	75	4.8	
1438+3135	14:38:24	31:35											6812			not detected
1443+2844	14:43:36	28:44	H	f13.	15	14.05	14.25	0.11	388	19	415	9200	9224	65	1.5	bright star nrby., sky uncertain, weak HI
I4504	14:44:24	31:55											9992			not detected
1447+2805	14:47:12	28:05											9627			not detected
I4514	14:48:42	27:46											9053			not detected
N5780	14:52:12	29:09											6984			not detected
1454+3141	14:54:48	31:41											9041			not detected
1502+2711	15:02:30	27:11		f13.	15				479	11		9293	9245		1.7	bad CCD data, repeat
1503+3121	15:03:30	31:21	H	f6.5	12	13.74	14.23	0.08	357	18	395	9998	9943	61	2.6	
1512+2647	15:12:24	26:47											9649			not detected
1519+3050	15:19:00	30:50											9239			not detected
N5924	15:19:54	31:24											9401			not detected
1522+3027	15:22:18	30:27											9357			too weak in HI
1528+2718	15:28:06	27:18											9700			not detected
1533+3058	15:33:18	30:58	H	f6.5	15	13.09	13.30	0.24	525	9	511	9438	9352	85	2.8	
1534+2729	15:34:06	27:29											9866			not detected
1536+2935A	15:36:40	29:35	–	f6.5	15	14.66	15.42	0.07	302	8	349	9785	9792	57	2.2	should have used f13.
I4568	15:38:00	28:19											9376			not detected
I4572	15:39:48	28:18		f13.	15	12.42	12.60	0.10				9791	9919	64		too weak and confused in HI

© American Astronomical Society • Provided by the NASA Astrophysics Data System

1992ApJ...395..347B

TABLE 2

DISTANCES AND PECULIAR VELOCITIES

Name	Sample	Distance Modulus	CMB Redshift	Peculiar Motion
N5672	...	33.35	3699	−986
N5639a	L	32.82	3707	36
N5709	L	32.89	3860	75
1426+3051	...	33.43	3983	−865
N5657	L	32.96	4059	143
1424+2145	L	32.67	4100	678
I4442	L	33.25	4354	−109
I4403	L	33.47	4443	−489
N5635	...	34.43	4446	−3259
N5641	L	33.24	4483	42
I4357	L	33.06	4526	436
1425+3010	L	33.41	4502	−306
1400+2816	L	33.47	4749	−185
N5166	P	33.65	4812	−566
N5263	P	32.96	4968	1065
1332+3141	...	34.34	5163	−2224
1313+3206	P	32.95	5245	1352
1318+3129	...	33.24	5226	784
1324+3228	P	33.62	5428	125
1320+3205	P	33.15	5507	1234
N5065	...	32.89	5691	1907
N5056	P	33.14	5734	1489
1314+3055	P	32.91	5814	1997
1312+3045	P	33.51	6186	1161
N5025	P	33.93	6494	381
1348+2824	*	33.98	7205	966
1405+3006	H	34.67	8380	−215
1343+2701	H	34.93	9100	−573
I4459	H	34.86	8982	−415
I4450	H	34.97	9236	−614
I4408	...	34.47	9229	1413
1443+2844	H	34.98	9342	−588
1533+3058	H	34.80	9602	486
1536+2935a	...	35.51	9941	−2701
1503+2131	H	34.78	10158	1125

because it is not contained in a well-defined structure. This omission has a negligible effect on the analysis.

3.2. *I-Band Tully-Fisher Relations*

Figure 3 shows the *I*-band TF relations for the galaxy * and for the samples H, L, and P. The magnitudes are the corrected isophotal magnitudes in column (8) of Table 1 and the corrected line widths are from column (12). Table 2 gives the best-fit slope and scatter for the three relations. Taken at face value, the scatter on the low-velocity edge (L) is larger than on the high-velocity edge (H). However, the low-velocity edge is composed of two groups differing by ~20% in both distance and redshift. The large scatter in sample P also suggests that these galaxies also have a significant range in distance.

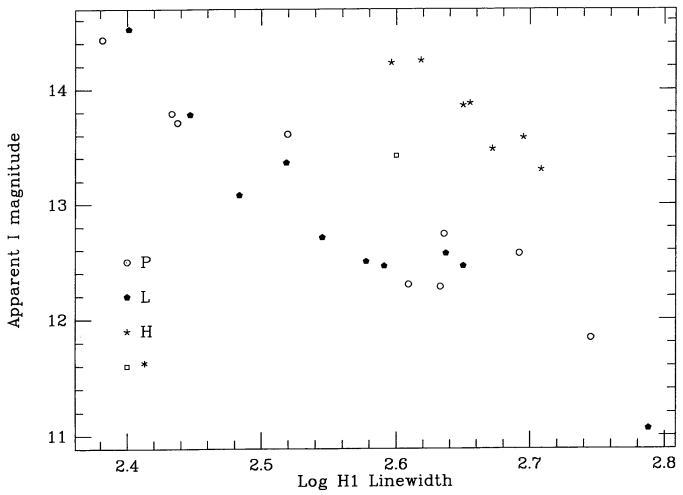

FIG. 3.—*I*-band TF relations for 27 galaxies

We compare our *I*-band TF relation with others in the literature. For the 15 "good" (i.e., normal surface brightness profile) galaxies in Bothun & Mould (1987) we derive a slope of -8.46 ± 0.60 with a scatter of 0.34 mag. Unfortunately, these data are on the Gunn *I* photometric system and the conversion from Gunn *I* to Cousins *I* is not well determined (e.g., its 0.65 ± 0.10 based on observations of standards in common). However, the uncertainty in the conversion affects only the zeropoint and not the slope of the *I*-band TF relation. Pierce & Tully (1988) published *I*-band magnitudes in the Cousins system. We impose an inclination cutoff of 45° on their data to derive a slope of -8.50 ± 1.11, $\sigma = 0.51$ mag for a sample of 20 galaxies in the Virgo cluster, -7.74 ± 0.98, $\sigma = 0.32$ mag for a sample of 16 galaxies in the Ursa Minor cluster, and -8.22 ± 0.76, $\sigma = 0.42$ mag for the combined sample. Because they are corrected for turbulence (see also discussion in Burstein & Raychaudhury 1989), Pierce and Tully's line widths are not reported according to the convention of Aaronson et al. (1980). This correction for turbulence primarily affects the

© American Astronomical Society • Provided by the NASA Astrophysics Data System

1992ApJ...395..347B

TABLE 3

IRTF RELATIONS

Subsample	Slope	Scatter
H.....	−8.7	0.113
	−8.5	0.114
L.....	−7.9	0.275
	−8.5	0.283
P.....	−6.5	0.276
	−8.5	0.372

zero point of the TF relation. Depending upon the actual distribution of line widths in the sample, it can also have a small effect on the slope. For example, Schommer, Bothun, & Williams (1991) derive a slope of -9.85 ± 0.7 using line widths corrected for turbulence compared with -9.02 ± 0.87 using the uncorrected values. The slopes of all of these relations agree within the errors: an unweighted mean gives -8.5 ± 0.35. In all of the following analysis we use this mean slope which is consistent with our data. Table 3 gives the scatter for our I-band TF relations with the slope constrained to -8.5.

Recall that our primary measurement is the relative distance between galaxies in sample H and sample L. Such a measurement requires only a consistent set of magnitudes and line widths for both samples and application of the same slope I-band TF relation to each sample (e.g., -8.5). Uncertainty in the true slope of the I-band TF relation introduces a small error in the determination of relative distances. For our sample, the mean distance modulus between samples H and L lies in the range $1.83 \pm 0.12 \leq \Delta(m - M) \leq 1.65 \pm 0.12$ for slopes in the range $-9.5 - -7.5$. Using a slope of -8.5 yields $\Delta(m - M) = 1.73 \pm 0.11$ mag. A potentially more serious systematic error arises if the I-band TF relation is *intrinsically* nonlinear. This is because of the significant difference in mean line width between galaxies in sample L compared to those in sample H. Use of a linear relation would then mean that sample H galaxies are systematically too faint with respect to the linear calibration while the sample L galaxies would be too bright. Nonlinearity in the TF relation observed by Aaronson (et al. 1986) is most likely an artifact resulting from the use of H-band aperture magnitudes instead of isophotal or total magnitudes. To date, all published I-band TF relations (e.g., Bothun & Mould 1987; Pierce & Tully 1988; Dressler & Faber 1990; Freudling, Martel, & Haynes 1991, Bothun et al. 1992) are highly consistent with linearity. In this case, the difference in mean line width between samples L and H introduces no bias as long as the same slope linear TF relation is applied to both samples. Equation (1) below fulfils this requirement.

3.3 *Maps of the Velocity Field*

We analyze the data in the frame where the average fractional peculiar velocity of the sample H + L is zero. Samples H and L have equal weight. In other words, we determine the normalization constant of the Tully-Fisher relation (with slope -8.5) which places the 17 galaxies on the Hubble flow. The internally calibrated I-band TF relation is

$$I_{\rm abs} = -19.73 - 8.5\,(\log \Delta V_c - 2.5)\,. \qquad (1)$$

Recall that we assume that this frame is also the one defined by the microwave background (CMB). The procedure we adopt precludes determination of translational motion of this sample. Table 2 lists the distance moduli and peculiar velocities relative to the CMD standard of rest for each galaxy.

Figure 4 shows the I-band TF relation which results from our internal calibration. Except for sample P (we show below that these galaxies are infalling toward Coma, see Fig. 5), the scatter is a remarkably small 0.18 mag, comparable with the error in an individual I-band TF measurement (Bothun & Mould 1987). Note that the absolute magnitudes are a function of the Hubble constant, but neither the slope nor the scatter depend upon the value of H_0.

The cone diagram in Figure 5*a* displays the data for all 35 galaxies with I-band TF distances. The circles indicate the redshift in the CMB frame. The lines are the line-of-sight velocity vectors. The circle is the *head* of the vector. Figure 5*b* is the same diagram for the 27 galaxies with reliable I-band TF measurements. Note that the six galaxies with the largest fractional peculiar velocities in Figure 5*a* have dropped out of the sample. Except for N5635 (§ 2.3), these large fractional peculiar velocities reflect errors in the data. Inclusion of these data would clearly bias the results toward "detection" of substantial flows. Thus some subjective quality control is quite important to avoid including galaxies with large errors caused by poor measurements, surface brightness incompatibility, and/or poorly determined inclination.

Figures 5*a* and 5*b* are maps in *velocity* space: we compare velocities predicted from the normalized TF relation with the measured redshifts. This comparison is independent of the Hubble constant.

Perhaps the most striking feature of the map (Fig. 5*b*) is that nearly all of the galaxies in sample P are falling toward Coma. If we include sample P in the determination of the reference frame, we still see infall. If sample P were stationary, sample H + L would be moving toward us at $\sim$400 km s^{-1}, a picture which makes less physical sense. In samples H and L there is no obvious flow.

3.4. *Photometric Diameter of the Void*

The cone diagram in Figure 1 shows sharply defined structure in redshift space. The measurement of peculiar velocities is necessary to understand the correspondence between structure in real space and that in redshift space. Despite the $\sim$5000 km s^{-1} diameter of the large void in redshift space, the correspon-

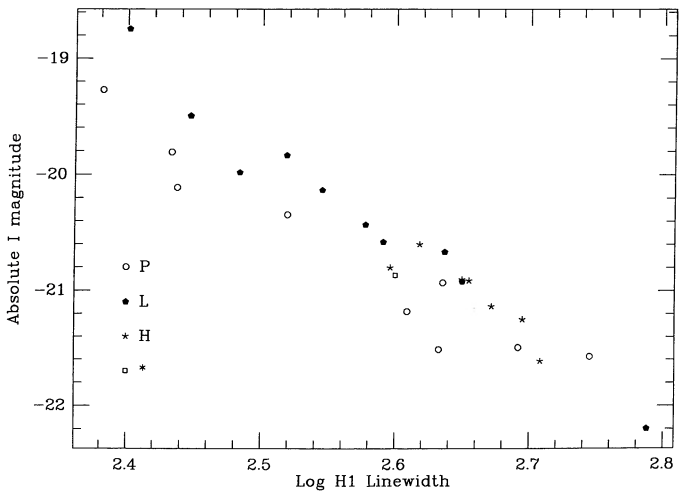

FIG. 4.—Internally calibrated TF relation for 27 galaxies

© American Astronomical Society • Provided by the NASA Astrophysics Data System

1992ApJ...395..347B

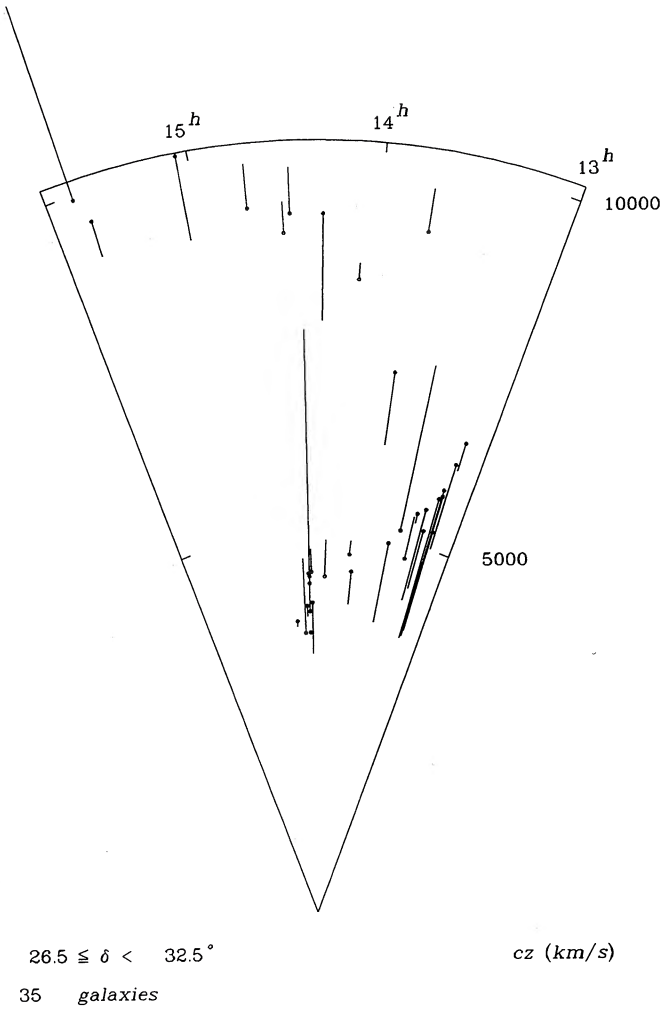

FIG. 5a

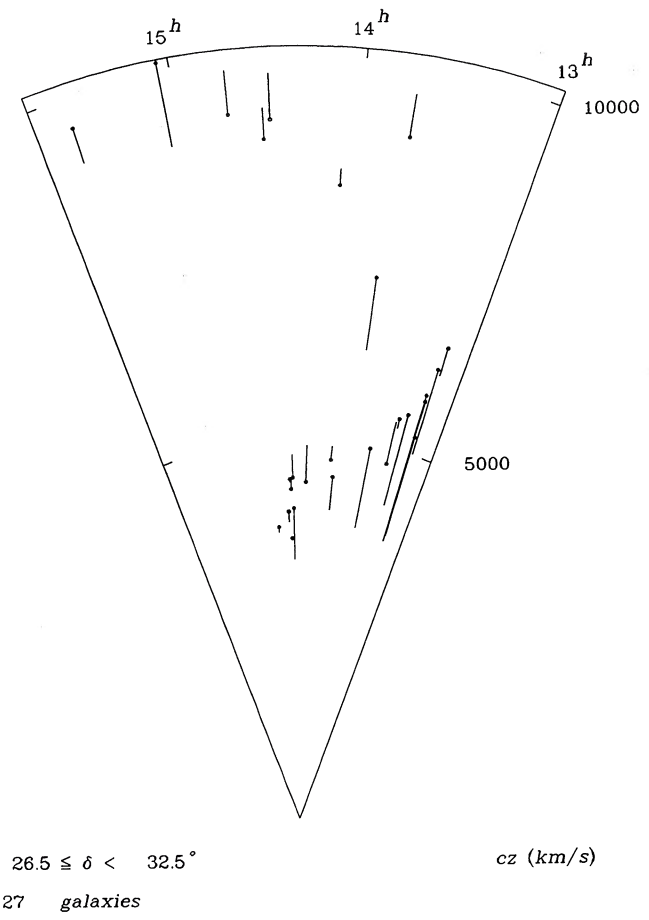

FIG. 5b

FIG. 5.—(*a*) Velocity field for the 35 galaxies with *I*-band TF measurements (α, , and *cz* areas in Fig. 1). The circle is the head of the arrow. (*b*) Velocity field for the 27 galaxies with reliable *I*-band TF distances. Note that the six largest vectors in Fig. 5*a* are absent from this sample. Also note the infall pattern toward Coma for the galaxies along the edge of the void at $\sim 13^h3$.

dence to a comparable feature in real space is not guaranteed a priori.

The data in Figure 5*b* provide a basis for a quantitative comparison. Samples H and L define the boundaries of the void. We can examine the correspondence between real and redshift space by assuming (1) the galaxies in group H (L) share an average peculiar velocity with respect to the Hubble flow or (2) the galaxies in group H (L) are all at the same distance. From case (1) we derive a limit on outflow from the void. In case (2) we compare the ratio of photometric distances with the ratio of velocities.

We can see the result for case (1) by looking at the map in Figure 5*b*. For both groups H and L the peculiar velocity vectors are randomly oriented indicating little, if any, flow. From the individual measurements listed in Table 2 we derive mean peculiar velocities of 32 ± 108 km s^{-1} for sample L and -113 ± 253 km s^{-1} for sample H. Both are obviously consistent with zero. Note that our procedure for defining the rest frame produces an approximately symmetric fractional outflow.

For case (2) we measure the offset between the Tully-Fisher relations for samples H and L in Figure 5*b* with slopes constrained to -8.5. The ratio of *I*-band TF distances is $2.22^{+0.11}_{-0.10}$ and the ratio of velocities in the CMB frame is 2.16 ± 0.08. In other words, to within the error the void has the same diameter in real and redshift space. We conclude that the 1 σ upper limit to outflow from the void is $\sim 5\%$ of the void diameter.

From calculations of the dynamics of isolated voids (Bertschinger 1985; Fillmore & Goldreich 1984), one might expect that we could calculate an upper limit to Ω from the limit on the outflow. However, simulations of the evolution of void-filled universes (Regös & Geller 1992) show that the flow velocity for a void boundary depends critically on its surroundings. If we had observed a large outflow velocity, we could conclude that Ω is large. For voids surrounded by other of comparable size, nature can conspire to produce outflow velocities consistent with zero for any $\Omega \lesssim 1$.

In the case at hand, we can only roughly estimate the diameters of the relevant surrounding voids. From the redshift survey in Figure 1 and from deeper data (Thorstensen et al. 1992), we estimate that the voids bounding the high (H) and low (L) velocity edges are, respectively, 1500 km s^{-1} and 4000 km s^{-1} smaller than the 5000 km s^{-1} void they enclose. A first approximation to the differential outflow velocity of an undis-

© American Astronomical Society • Provided by the NASA Astrophysics Data System

1992ApJ...395..347B

turbed wall (between identified voids) is

$$v_{\rm out} \sim 0.1 H_0 (d_1 - d_2) \Omega^{0.6} , \quad (2)$$

where d_1 and d_2 are the diameters of the adjacent voids along the direction perpendicular the wall (Regös & Geller 1992). We assume that the galaxies trace the matter distribution.

The 2 σ limits on outflow for samples H (-113 ± 253 km s^{-1}) and L (32 ± 108 km s^{-1}) then yield $\Omega \lesssim 1$. Here we have ignored the effect of Malmquist bias because its application in a highly clustered universe is ambiguous (see Landy & Szalay 1992). Application of the General Malmquist correction, as formulated by Landy & Szalay (1992) requires a continuous distribution of distances. From this distribution, one then determines the probability that the observed structures along the line of sight, when combined with distance errors, serves to scatter points to systematically larger *or* smaller distances (see Bothun et al. 1992). Our sample, however, does not exhibit a continuous distribution of distances (because there is a large-scale void) and hence we can not employ the Landy and Szalay correction. However, the Malmquist correction is largely irrelevant in our case. We are essentially dealing with two *isolated* structures ("sheets"); there are no other structures along the line of sight where distance errors would cause interlopers to be erroneously assigned to samples L or H. Indeed, the distance measurements themselves indicate that galaxies in samples L and H are at the same distance. Since this is equivalent to working in a galaxy cluster, a Malmquist correction is not required.

3.5. *Infall Toward Coma*

Considering Figure 5*b* again, we note that the velocity vectors for eight of the nine galaxies in sample P point in the same direction (away from the origin). The most natural interpretation of this flow is that these galaxies are falling into the Coma cluster. We detect infall at the $\gtrsim 3$ σ level and we derive an estimate of Ω from the relation

$$v_{\rm pec}/H_0 r \sim \Omega^{0.6} p(\Delta) \quad (3)$$

(Regös & Geller 1992) where $v_{\rm pec}$ is the peculiar velocity and Δ is the average density enhancement inside radius r.

The mean position of sample *P* is $\alpha = 13^{\rm h}19^{\rm m}8^{\rm s}$, $\delta = 31\overset{\circ}{.}39$, and $cz = 5576 \pm 181$ km s^{-1} (CMB frame). For the mean position of Coma we take $\alpha = 12^{\rm h}57^{\rm m}10^{\rm s}$, $\delta = 28\overset{\circ}{.}23$, $cz = 7235 \pm 50$ km s^{-1} (CMB frame). The separation in redshift space is 1679 ± 190 km s^{-1}. The *I*-band TF data yield an infall velocity for sample *P* (component along the line-of-sight) of 915 ± 263 km s^{-1}. Then $v_{\rm pec}/H_0 r \simeq 0.36$ at a separation of $26\ h^{-1}$ Mpc. This $\gtrsim 3$ σ detection is conservative. We omitted the two galaxies N5065 and 1318 + 3129 from the sample because of their uncertain inclinations. Including these galaxies yields an infall of 993 ± 232 km s^{-1}.

We obtain the density enhancement Δ for Coma by extrapolating the surface density profile ($\rho \propto r^{-2}$) based on the 210 galaxies with $m_{B(0)} \leq 15.5$ within the central $5\overset{\circ}{.}5$ of the cluster (Regös & Geller 1992). We assume once again that the galaxies trace the large-scale matter distribution. We obtain $\Delta = 0.8$ which yields $\Omega = 2.2^{+20}_{-2}$ (2 σ error).

Even these large error limits are surely an underestimate; they include only the error in the computed infall velocity and ignore the large uncertainty in Δ. Furthermore the spherically symmetric model is obviously inadequate. The interpretation of the "infall" velocity is complicated by the confinement of most of the galaxies to thin sheets. For a void diameter of 5000 km s^{-1} streaming velocities along the wall are of the order of 1000 km s^{-1} $\Omega^{0.6}$ (Regös & Geller 1992). The contribution of these streaming velocities to the measured infall depends upon the detailed dynamics of the system; they may well be responsible for the large value we derive for Ω in the naive model.

If we ignore the streaming velocities and assume that the motion is all caused by infall to Coma, we predict that sample L should be infalling toward Coma at ~ 560 km s^{-1}. Outflow from the void should compensate the expected infall, but computation of a complete, internally consistent model is beyond the scope of this paper (and is not warranted by the amount of data in hand so far).

4. CONCLUSIONS

Dense redshift surveys now cover a substantial fraction of the nearby universe (see e.g., Geller & Huchra 1989; da Costa et al. 1988; Haynes & Giovanelli 1986). However, full physical interpretation of these data requires that we measure distances to individual galaxies as well as their redshifts. In a region covered by a complete redshift survey, the distance estimates are important for limiting the distortions of redshift relative to real space and for understanding the dynamics of the region.

The analysis of a sample of distance measurements coupled with a redshift survey is subtle. The well-known Malmquist bias depends upon the actual spatial distribution of objects (Landy & Szalay 1992) and may not be relevant in the case of isolated "sheets" of galaxies. The expected line-of-sight peculiar motions are sensitive to the orientation of the spatial structure ("walls") relative to the line of sight (Regös & Geller 1992). For example, streaming velocities along "walls" can easily be confused with bulk motions. A complete redshift survey in the region is necessary even for even a rudimentary analysis. With a total of 27 reliable distance measurements we are able to show that:

1. The ratio of *I*-band TF distances to the high- and low-velocity boundaries (samples H and L) is $2.22^{+0.11}_{-0.10}$ and the ratio of velocities of 2.16 ± 0.08. In other words, to within the error the void has the same diameter in real and redshift space. These ratios are insensitive to the definition of the standard of rest.

2. The mean peculiar velocity of sample L is 32 ± 108 km s^{-1}; for sample H it is -113 ± 253 km s^{-1}. In other words, the data are consistent with no outflow from the void and the 1 σ upper limit to outflow from the void is $\sim 5\%$ of its diameter. This limit is more stringent than the earlier limit by Freudling et al. (1988) because of the smaller scatter in the *I*-band Tully-Fisher relation. A simple model for the outflow yields a 2 σ on $\Omega \lesssim 1$. The small velocities are reassuring because it would otherwise be difficult to understand why the structures are so sharp in redshift space.

3. Finally, we detect the "infall" of sample P toward Coma: the line of sight component of the infall is 915 ± 263 km s^{-1} on a scale of $26\ h^{-1}$ Mpc. This detection provides one of the largest scale dynamical measurements of Ω with admittedly large and poorly determined error. We estimate $\Omega = 2.2^{+20}_{-2}$ where the error is only the formal 2 σ error resulting from the error in the infall velocity alone. The large value of Ω obtained in our simple spherically symmetric model probably reflects the importance of streaming motions along the wall.

Within the 2 σ error limits, the data do allow a consistent simple picture for both the infall and the outflow from the void

© American Astronomical Society • Provided by the NASA Astrophysics Data System

1992ApJ...395..347B

(for $0.2 \lesssim \Omega \lesssim 1$). However the structure is sufficiently complex that detailed modeling beyond the scope of this paper is required. Sampling the "Great Wall" over its entire extent at the density of the sample in this paper would substantially improve the constraints and we are planning to obtain such a sample in the near future.

We thank Enikö Regös for helpful discussions and for calculations of Δ. We thank Robert K. McMahan for compiling the photometric data. We thank Ann Zabludoff for helping to prepare Table 1. This research is supported in part by NASA grant NAGW-201 and by the Smithsonian Scholarly Studies Program.

REFERENCES

Aaronson, M., Bothun, G., Mould, J. R., Huchra, J. P., Schommer, R. A., & Cornell, M. E. 1986, ApJ, 302, 536
Aaronson, M., Huchra, J. P., Mould, J. R., Schechter, P. L., & Tully, R. B. 1982, ApJ, 258, 64
Aaronson, M., Huchra, J. P., Mould, J. R., Sullivan, W., Schommer, R., & Bothun, G. 1980, ApJ, 239, 12
Aaronson, M., et al. 1989, ApJ, 338, 654
Bertschinger, E. 1985, ApJS, 58, 1
Boroson, T. 1981, ApJS, 46, 177
Bothun, G. D., Aaronson, M., Schommer, R., Mould, J. R., Huchra, J. P., & Sullivan, W. 1985, ApJS, 57, 423
Bothun, G. D., & Cornell, M. E. 1990, AJ, 99, 1004
Bothun, G. D., & Mould, J. R. 1987, ApJ, 313, 629
Bothun, G., & Rogers, C. 1992, AJ, 103, 1481
Bothun, G. D., Schommer, R. A., Williams, T., & Mould, J. R. 1992, ApJ, 388, 253
Burstein, D., Davies, R., Dressler, A., Faber, S., Stone, R., Lynden-Bell, D., Terlevich, R., & Wegner, G. 1987, ApJ, 318, 944
Burstein, D., & Raychaudhury, S. 1989, ApJ, 343, 18
Cen, R. 1992, ApJ, submitted
Centrella, J. M., Gallagher, J. S., Melott, A. L., & Bushouse, H. A. 1988, ApJ, 333, 24
Cowie, L. L., & Ostriker, J. P. 1981, ApJ, 243, 427
da Costa, L. N., Pellegrini, P. L., Sargent, W. L. W., Tonry, J., Davis, M., & Meiksin, A. 1988, ApJ, 327, 544
de Lapparent, V., Geller, M. J., & Huchra, J. P. 1986, ApJ, 302, L1
Disney, M., Davies, J., & Phillips, S. 1989, MNRAS, 239, 939
Dressler, A. D., & Faber, S. M. 1990, ApJ, 354, 13
Fillmore, J. A., & Goldreich, P. 1984, ApJ, 281, 9
Freedman, W. 1990, ApJ, 335, L35
Freudling, W., Haynes, M. P., & Giovanelli, R. 1988, AJ, 96, 1791
Freudling, W., Martel, H., & Haynes, M. P. 1991, ApJ, 377, 349
Geller, M. J., & Huchra, J. P. 1989, Science, 246, 879
Giovanelli, R., Haynes, M. P., Rubin, V. M., & Ford, W. 1986, ApJ, 301, L7
Halpern, M., Benford, R., Meyer, S., Muehlner, D., & Weiss, R. 1988, ApJ, 332, 996
Haynes, M. P., & Giovanelli, R. 1986, ApJ, 306, L55
Huchra, J. P., Geller, M. J., de Lapparent, V., & Corwin, H. G. 1990, ApJ, 72, 433
Ikeuchi, S. 1981, PASJ, 33, 211
Landolt, A. U. 1983, AJ, 88, 439
Landy, S., & Szalay, A. 1991, 1992, ApJ, 391, 484
Lynden-Bell, D., Faber, S. M., Burstein, D., Davies, R. L., Dressler, A., Terlevich, R. J., & Wegner, G. 1988, ApJ, 326, 19
Marzske, R., et al. 1992, in preparation
Park, C. 1990, MNRAS, 242, 59P
Pierce, M. J., & Tully, R. B. 1988, ApJ, 330, 579
Readhead, A. C. S., Lawrence, C. R., Myers, S. T., Sargent, W. L. W., Hardebeck, H. E., & Moffet, A. T. 1989, ApJ, 346, 566
Regös, E., & Geller, M. J. 1989, AJ, 98, 755
———. 1992, ApJ, in press
Rubin, V. M., Burstein, D., Ford, W., & Thonnard, N. 1985, ApJ, 289, 81
Saunders, W., et al. 1991, Nature, 349, 32
Schild, R. E. 1983, PASP, 95, 1021
Schombert, J. M., Bothun, G., Schneider, S. E., & McGaugh, S. S. 1992, AJ, 103, 1107
Schommer, R., Bothun, G. D., & Williams, T. 1991, preprint
Thorstensen, J. R., et al. 1992, in preparation
Tonry, J. L., & Davis, M. 1981, ApJ, 246, 680
Valentjin, E. 1990, Nature, 346, 153
Villumsen, J. V., & Davis, M. 1986, ApJ, 242, 448
Weinberg, D. H., & Gunn, J. E. 1990, ApJ, 352, L25
White, S. D. M., Frenk, C. S., Davis, M., & Efstathiou, G. 1987, ApJ, 313, 505
Witt, W., Thronson, H., & Capuano, J. 1991, preprint
Yahil, A. 1985, in The Virgo Cluster of Galaxies, ed. O.-G. Richter & B. Binggeli (Garching: ESO)

© American Astronomical Society • Provided by the NASA Astrophysics Data System